Activatable probes for diagnosis and biomarker detection by MRI

Monica Carril

CIC biomaGUNE, Paseo Miramón 182, 20009 Donostia - San Sebastian, Spain.

Ikerbasque, Basque Foundation for Science, 48011 Bilbao, Spain.

E-mail: mcarril@cicbiomagune.es

Keywords. Responsive-probes, OFF/ON probes, activatable probes, MRI, ^{19}F MRI

Abstract: Magnetic resonance imaging (MRI) is a non invasive imaging technique with widespread use in diagnosis. Frequently, contrast in MRI is enhanced with the aid of a contrast agent, among which smart, responsive, OFF/ON or activatable probes are of particular interest. These kinds of probes elicit a response to selective stimuli, evidencing the presence of enzymes or acidic pH, for instance. In this review, we will focus on smart probes that are detectable by both ^{1}H and ^{19}F MRI, frequently based on nanomaterials. We will discuss the triggering factors and the strategies employed thus far to activate each probe.

1. Introduction.

Magnetic resonance imaging (MRI) is a non invasive imaging technique with widespread use in diagnosis due to its good spatial resolution and acceptable sensitivity. Frequently, contrast in MRI is enhanced with the aid of a probe or contrast agent. It is often distinguished between T_1 and T_2 contrast agents, that is, those that either brighten or darken images, respectively. Those contrast agents function by altering the longitudinal or transverse relaxation times of surrounding water within the body. Among existing contrast agents, smart or activatable

probes are of particular interest. These kinds of contrast agents elicit a response to selective stimuli, evidencing the presence of active enzymes, acidic pH or reducing environments, for instance. In an ideal situation, we would go from a non-detectable probe (OFF state) to a detectable probe (ON state) due to a selected trigger. Indeed, there are a number of pure OFF/ON contrast agents, but in many other examples, the starting point is not a completely OFF state, but a situation in which MRI signal is relatively low, and upon contact with the trigger the probe properties are significantly altered and a substantial increase of contrast is detected. By the use of smart or activatable probes it is possible to gain information about dynamic processes and obtain functional information in real time which can help to make a more specific diagnosis. All these types of probes are known as activatable, OFF/ON, smart or (bio)responsive, but they all fall into the same definition since they react to external stimuli.

In this review, we will focus on smart probes that are detectable by MRI and we will do a first classification to discuss proton based MRI (^{1}H MRI) probes and fluorine based MRI (^{19}F MRI) probes, frequently based on nanomaterials. Within each type of probe we will also classify them according to the triggering factor. We will in addition discuss the mechanisms and strategies inherent to the composition of the probe, which have been employed thus far to turn OFF and ON each kind of probe exposed to each kind of environment. For the case of ^{1}H MRI probes there have been several reviews published in the last years which discuss smart probes for imaging in general[1-4] and also for MRI in particular,[5-12] hence we will only focus on the most recent examples, mostly from 2014 onwards. On the contrary, activatable ^{19}F MRI will be discussed in more detail since they have been less extensively revised.[1, 13]

2. Activatable probes for ^{1}H MRI.

There are different mechanisms to take into account when building activatable probes for ^{1}H MRI based on the intrinsic nature and behaviour of each type of contrast agent. For the case of

T_1 contrast agents,[12] a common strategy is to modulate their relaxivity (r_1) by hampering the accessibility of water to the coordination sphere of the paramagnetic metal (Gd (III) most frequently).[9] This shielding effect reduces the r_1 value so that the probe is mostly undetectable. Once the access to water molecules is restored, r_1 increases significantly leading to much brighter images. Also, the tumbling rate can be controlled by attaching/detaching the probe from a rigid support and modulate in this manner the r_1 value. In other examples, the external trigger leads to increased accumulation of the probe at the site of the trigger presence and hence, the contrast is locally increased. Manganese based T_1 contrast agents are frequently used as bioresponsive probes because they are administered in the form of Mn (III) or (IV) salts and the T_1 contrast is turned ON by the release of Mn^{2+} cations by different triggers, usually in acidic and reducing environments. Much less examples of activatable probes have been described with T_2 contrast agents and are based on the release of encapsulated iron oxide nanoparticles (NPs) or on induced accumulation of probe, for instance by precipitation. We will discuss the probes with respect to the trigger that activates them. A table summary is included with all the examples that will be described collecting the trigger, its consequence, the effect observed by MRI (or nuclear magnetic resonance (NMR) in some preliminary studies) and if they have been tested in solution, cells or *in vivo* (Table 1).

Table 1. Summary of ^{1}H MRI activatable probes.

	Probe	Enzyme and consequence	Effect observed	Application	Ref.
Enzyme- responsive probes	EGad (Gd - galactopyranose)	β-galactosidase: Probe ligand cleavage	Increased T_1 contrast.	Proof of concept in solution	14
	Gadoteridol @ liposomes	PLA_2: Liposome rupture and probe release	Increased T_1 contrast.	Proof of concept in solution	15
	C-SNAM (Gd)	Caspase-3: Probe self assembly and nanoaggregation leading to increased tissue retention	Increased T_1 contrast.	Stem cell apoptosis imaging. *In vitro* and *in vivo*.	16
	C-SNAM (Gd)	Caspase-3/7: Probe self assembly and nanoaggregation leading to increased tissue retention	Increased T_1 contrast.	Drug induced tumour death *in vitro* and *in vivo*	17
	Gd - peptide	PDI based probe activation leading to fibrin binding in new blood clots	Increased T_1 contrast	Proof of concept in solution	18
	Mn (III)-porphyrins	SEAP: Porphyrin cleavage leading to insoluble product. Probe accumulation at enzyme site.	Increased T_1 contrast.	Gene mapping. *In vitro*, ex vivo and *in vivo*.	19
	CLIO - ICT (Fe)	MMP-14: ICT peptide conjugate cleavage. Probe accumulation at enzyme site.	Increased T_2 contrast.	MMP-14 imaging, *in vitro* and *in vivo* in a breast cancer mouse model.	20
	Ln (III) complex-β-D-galactopyranoside	β-galactosidase: Probe ligand cleavage	Increased r_1 (Gd3+). PARACEST response turned off (Yb3+)	Proof of concept in solution	21
	ZGGR-α-amino-(Tm-DOTA)	uPA: ZGGR peptide ligand cleavage.	Fast disappearance of CEST effect	*In vivo* pancreatic tumour model.	22
	PLG	Cathepsins: probe cleavage	CEST signal differences	*In vitro* and *in vivo* in a brain cancer model	23
pH-responsive probes	**Probe**	**pH consequence**	**Effect observed**	**Application**	**Ref.**
	MnO @ SiO_2	Release of Mn^{2+} by dissolution of MnO	Increased T_1 contrast	*In vitro* imaging of cancer cells	24
	SiO_2 @ $MnSiO_3$	Release of Mn^{2+} by dissolution of $MnSiO_3$	Increased T_1 contrast	*In vitro* and *in vivo* imaging of cancer.	25
	Mn @ CaP NPs	CaP NP disintegration and release of Mn^{2+} which bind to proteins	Increased T_1 contrast	*In vivo* tumour hypoxia imaging	26
	$MnAsO_x$ @ SiO_2	Release of Mn^{2+}	Increased T_1 contrast	*In vitro* and *in vivo* drug delivery imaging in tumours	27
	Gd-DOTA-dendrimer	Protonation of dendrimer affects proton exchange with Gd	Increased r_1 at pH < 6.35 Unmodified r_2	R_2/R_1 ratio allows calculating pH accurately and independently from concentration. Proof of concept in solution	28
	Gd @ SiO_2-polymer	Polymer morphological changes (shrinkage at lower pH)	Increased r_2 at pH < 7 Unmodified r_1	Proof of concept in solution	29
	Gd NPs @ polymer	Polymer coating swelling and hydrolysis	Increased r_1 at pH < 7	Proof of concept in solution	30
	Gd @ polymeric NPs	Polymer coating shrinkage. Probe accumulation at acidic sites	Increased T_1 contrast	*In vivo* tumour imaging.	31
	Gd NPs + polymer	Induced conformational changes in polymers.	Increased r_1 at pH < 7	Proof of concept in solution	32
	Fe_3O_4 NPs @ micelles	Micelle disassembly and Fe_3O_4 NPs release	Increased T_2 contrast when pH < 6.8	pH measurement *in vivo* in an ischemic model.	33

Table 1. Summary of ^{1}H MRI activatable probes (continuation).

	Probe	Redox consequence	Effect observed	Application	Ref.
Redox responsive probes	Fe_3O_4@Mn_3O_4	Release of Mn^{2+} by GSH Release of Fe_3O_4	Increased T_1 contrast (Mn) Increased T_2 contrast (Fe)	*In vitro* and *in vivo* imaging of cancer	34
	MnO_2 nanosheets	Release of Mn^{2+} by GSH	Increased T_1 contrast	*In vitro* and *in vivo* cancer imaging	35
	MnO_2 nanosheets	Release of Mn^{2+} by GSH	Increased T_1 contrast	*In vitro* tumour cells imaging	36
	SiO_2 @ $MnSiO_3$	Release of Mn^{2+} by GSH	Increased T_1 contrast	*In vitro* and *in vivo* imaging of cancer.	25
	Mn chelates	Production of Mn (II) from Mn (III) chelated in reducing environment	Increased r_1	Proof of concept in solution	37
	Mn chelate	Reversible Mn (III) / Mn (II) production in the presence of either GSH or H_2O_2.	Increased r_1 when Mn (II) is produced	Proof of concept in solution	38
	Cu	Reversible Cu (I) / Cu (II) production in the presence of either reductants or oxidants.	Variations in r_1	Proof of concept in solution	39
	Gd chelate – SiO_2 NPs	Release of Gd chelates by GSH	Increased T_1 contrast	Proof of concept in solution	40
	Gd chelates	Intramolecular macrocyclization to form Gd NPs	Increased r_1	*In vitro* detection of reducing environments (GSH)	41
	Gd – polymer - peptides	Release of peptides and increased exposure of Gd	Increased r_1	Proof of concept in solution	42
Ion-responsive probes	**Probe**	**Ion and reaction**	**Effect observed**	**Application**	**Ref.**
	Gd chelates	Ca^{2+} binding	Increased r_1	*In vitro* detection of intracellular Ca^{2+}	43
	Gd chelates	Ca^{2+} binding	Increased r_1	*In vitro* detection of intracellular Ca^{2+}	44
	Gd chelate	Ca^{2+} binding	Increased r_1	Proof of concept in solution	45
	Gd - dendrimer	Ca^{2+} binding	R_1/R_2 ratio variation	Proof of concept in solution	46
	Gd chelate	Cu^{1+} binding	Increased r_1	*In vitro* copper accumulation in Menkes disease.	47
Other probes	**Probe**	**Trigger and consequence**	**Effect observed**	**Application**	**Ref.**
	Gd-DTPA @ liposomes	Cocaine: release of DNA-PLA_2 leading to liposome degradation and probe release	Increased T_1 contrast.	Cocaine detection. Proof of concept in solution	48

Abbreviations: Egad: (4,7,10-tri(acetic acid)-l-(2-β-galactopyranosylethoxy)-1,4,7,10-tetraazacyclododecane)gadolinium; C-SNAM: caspase-3-sensitive nanoaggregation MRI probe; CLIO: cross-linked iron oxide; ICT: azademethylcolchicine; DOTA: 1,4,7,10-tetraazacyclododecane-1,4,7,10-tetraacetic acid; PLG: poly-L-glutamate; DTPA: diethylenetriaminepentaacetic acid; PLA_2: phosphatidylcholine 2-acetylhydrolase; PDI: protein disulfide isomerise; SEAP: secreted alkaline phosphatise; MMP: matrix metalloproteinase; uPA: urokinase plasminogen activator; CEST: Chemical Exchange Saturation Transfer. GSH: glutathione. @ = encapsulated in.

2.1. Enzyme-responsive ^{1}H MRI probes.

The study of enzymatic activity by MRI is one of the main areas of interest in the field of activatable probes, since enzyme dysregulation is in itself a symptom of disease. Not only their sole presence in active form is a biomarker of several types of cancer but they can also be an indicator of the state of progression of many pathologies, such as atherosclerosis. Since the seminal work of Moats et al. using a β-galactosidase responsive Gd (III) chelate (Egad),[14] there has been an increasing interest in developing enzyme-responsive probes and several reviews cover the literature of the last decades.[4, 6] Herein, as mentioned in the introduction, we will mostly discuss examples of the last two years.

Caspase-3/7 is an enzyme that plays an essential role in cell apoptosis. It is of interest in cancer research since radio and chemotherapy-induced cell death is often based on caspase-3/7 activation in tumours. Hence, its activity provides valuable information regarding the tumour therapeutic response to drugs. Rao and co-workers[17] have extended their controlled self assembly and macrocyclisation strategy to form Gd NPs with amplified r_1 upon contact with caspase-3/7. This is achieved by the increase of tumbling rate when Gd complexes are assembled into such NPs. For this purpose, they synthesised a probe named by them as C-SNAM consisting of a Gd-DOTA complex linked to a DEVD peptide recognised by the enzyme, a disulfide bond sensitive to glutathione (GSH) and the required moieties for the self-assembly, that is a 2-cyano-6-hydroxyquinoline and a D-cysteine residue. The cyclisation was triggered by the DEVD peptide degradation in the presence of caspase-3/7 in a reducing environment (intracellular presence of GSH) which led to an enhancement of the T_1 contrast in MRI due to the r_1 amplification in the Gd NPs and tissue retention as a result of the size increase. They successfully applied this probe to *in vitro* and *in vivo* imaging of caspase-3/7 activity in a chemotherapy responsive tumour model and compared it to a probe that could not undergo cyclisation (Figure 1). In another study, the same probe and strategy was used to detect stem

cell apoptosis following intra-articular injection of matrix-associated stem cell implants (MASI), which is envisaged as a promising therapy for cartilage defects.[16]

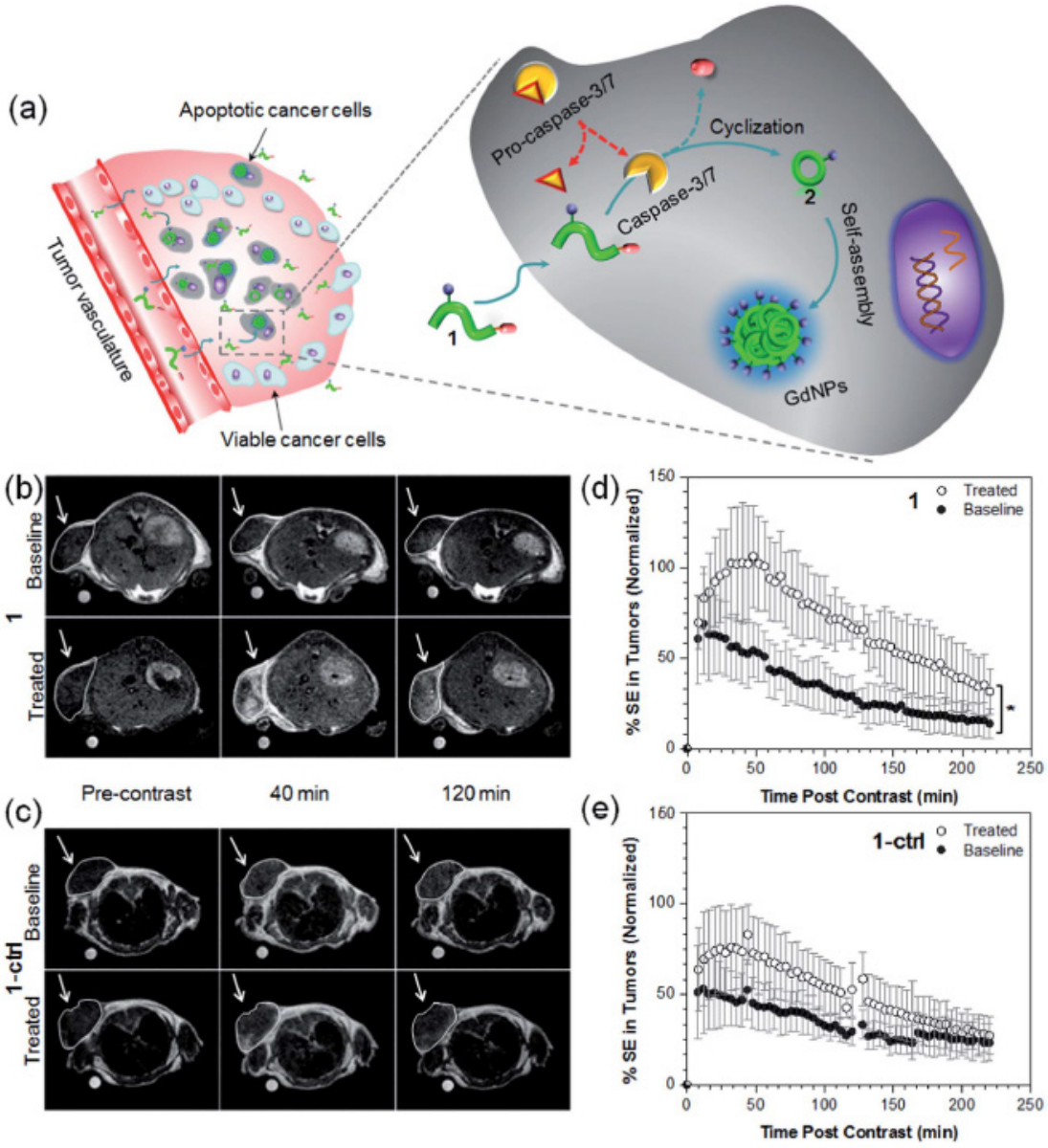

Figure 1. Non-invasive MR imaging of tumour cell death in mice. A) The proposed mechanism for in vivo MR imaging of caspase-3/7 activity. (B and C) Representative T1-weighted MR images of tumors prior to (baseline) or following treatment with DOX (treated), and after injection of activatable probe (B) or control probe (C). (D and E) The average longitudinal % signal enhancement (% SE). Reproduced from Ref. 17 with permission from The Royal Society of Chemistry.

Loving and Caravan[18] reported a probe to detect fresh blood clots to prevent thrombosis based on the activity of protein disulfide isomerase (PDI), which is a biomarker of newly formed blood clots since it appears in its active form on the surface of activated platelets. They designed a Gd chelate functionalized with a fibrin targeted peptide and specifically located disulfide moieties that could be modified by PDI. When the probe was exposed to PDI, it hydrolysed the disulfide bonds to form a new intramolecular disulfide bond and induced a conformational change in the peptide that was then able to bind fibrin, which is also abundant in blood clots, enhancing probe retention in the clot. The authors observed a 70 % increase in r_1 when the probe was bound to fibrin. Older clots lack active PDI and hence no probe retention would take place.

Changes in PLA_2 activity have been suggested as a biomarker for several pathologies such as atherosclerosis, acute sepsis, prancreatitis and some types of cancer. Hence, Cheng et al.[15] took advantage of the PLA_2 triggered degradation of glycerophospholipids to detect its activity by loading liposomes with gadoteridol, a Gd chelate. When gadoteridol was encapsulated, the T_1-weighted signal was low due to the reduced permeability of the liposomes that hampered the water molecule accessibility. In the presence of PLA_2, liposomes were degraded and the Gd probe released leading to a substantial decrease in T_1 relaxation time.

Westmeyer et al.[19] proposed an MRI-based gene mapping methodology by using a probe responsive to reporter enzyme secreted alkaline phosphatise (SEAP). They prepared a probe consisting of a water soluble modified porphyrin chelate with Mn (III), based on previously reported porphyrin structures that were cleavable by SEAP. Upon enzymatic degradation the water soluble manganese probe turned insoluble, accumulated at the site where the enzyme was present and T_1 contrast increased accordingly.

In addition to T_1 contrast agents, T_2 imaging probes have also been used as activatable probes taking advantage of the activity of selected enzymes. Ansari et al.[20] reported the design and

characterisation of a matrix metalloproteinase 14 (MMP-14) responsive probe based on iron oxide NPs functionalised with a MMP-14 targeting peptide. At tumour sites, MMP-14 cleaved the peptide leading to increased and selective probe accumulation in tumour and hence an enhancement of T_2 contrast agent was observed when compared with the non-targeted probe (without peptide). They also used this probe as a drug delivery system for therapy in a breast cancer rodent model.

Other enzyme responsive examples used lanthanide (III) complexes as Chemical Exchange Saturation Transfer (CEST) imaging agents. For instance, He et al.[21] monitored the activity of β-galactosidase through the turn-off of CEST effect in the presence of such enzyme. A similar strategy was used by Yoo et al.[22] to monitor urokinase plasminogen activator (uPA) by detecting the disappearance of CEST signal in the presence of uPA *in vivo*. The group of Reddy[23] used poly-L-glutamate (PLG) as a CEST probe to detect cathepsins activity in cancer. This family of enzymes are usually over-expressed in tumour cells. In this work, cathepsins cleaved the probe and induced differences in CEST signal between the cleaved and uncleaved PLG. This system was validated *in vitro* and *in vivo* in a brain tumour model and was proposed as a diagnosis tool.

2.2. pH-responsive ^{1}H MRI probes.

It is known that pH values are lower in tumour cells compared to healthy cells. Hence, researchers in the field have pursued the design of probes to detect acidic pH, particularly in the approximate range of 5.5 to 6.8, because it is considered a cancer biomarker.[49] Probes responsive to acidic pH work basically in two manners, they are either degraded and cations active in MRI are released to the medium, or a morphological change is induced by shrinkage/swelling of the probe or by disassembly.

Manganese based probes are frequent for pH detection. Manganese inorganic compounds are able to release Mn^{2+} cations in acidic pH. This process is usually favoured in reducing environments, like those in tumour cells, as it will be discussed in the following section (redox responsive probes). Mn^{2+} cations are active as T_1 contrast agents and are emerging in the last years as an interesting substitute for Gd^{3+} due to its reduced toxicity compared to Gd (III). These are OFF/ON agents that turn on their signal at pH values below 7. The groups of Nishiyama and Kataoka[26] produced calcium phosphate (CaP) NPs with Mn (II) cations encapsulated, which they named as PEGMnCaP. Such CaP NPs were dissolved in acidic pH and the released Mn (II) ions bound to proteins leading to a substantial increase in T_1 contrast. The authors demonstrated that solid tumours could be rapidly imaged by these NPs (Figure 2), and that they were able to detect hypoxic regions within tumours as well as really small metastatic tumours in the liver.

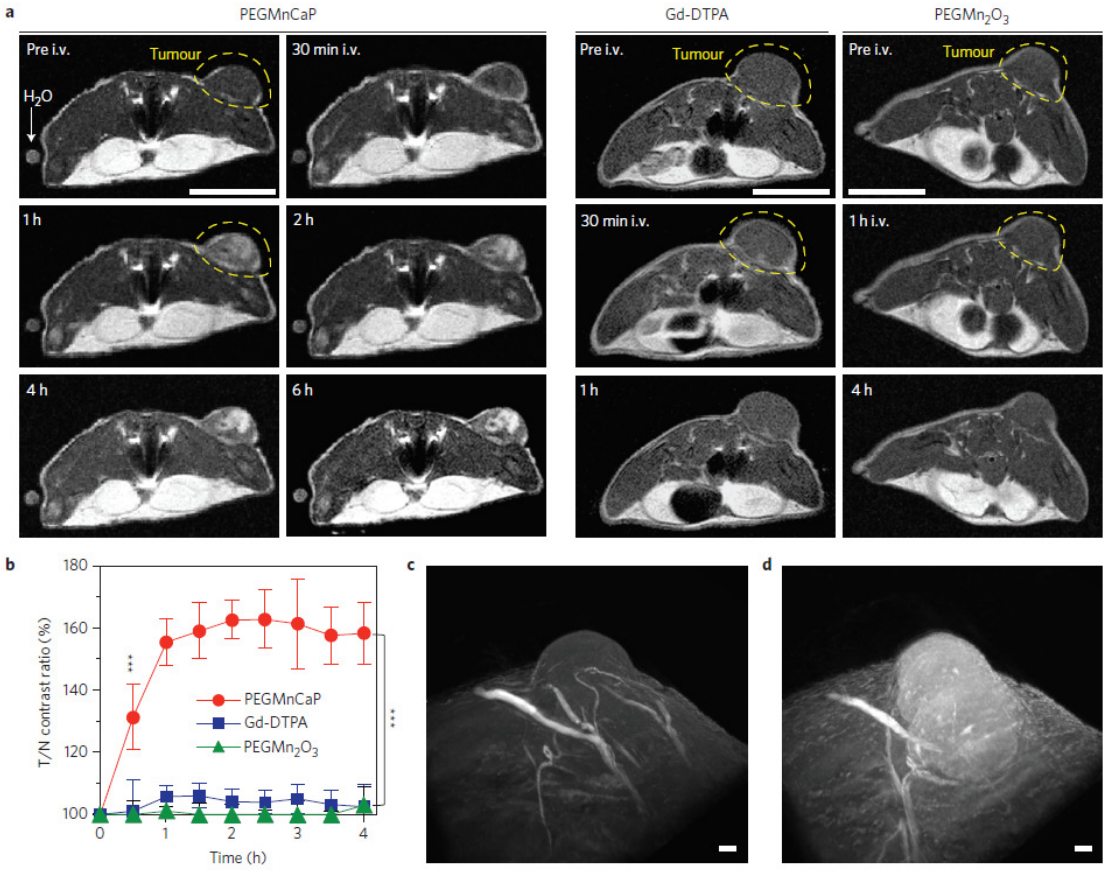

Figure 2. A) In vivo MR images of tumour-bearing mice pre- and post-intravenous injection of PEGMnCaP (left) and control probes (Gd-DTPA and $PEGMn_2O_3$), showing selective and high enhancement of tumour contrast only for PEGMnCaP. B) Tissue to Noise (T/N) contrast ratio after the administration of all probes. C) and D) 3D MRI of tumours before (C) and 1 h after (D) the intravenous injection of PEGMnCaP. Reprinted by permission from Macmillan Publishers Ltd: Nature Nanotechnology 11, 724–730, copyright (2016) (Ref. 26).

Zhao et al.[27] designed a smart probe which acted both as a drug for therapy and as an imaging agent. They loaded silica NPs with arsenic trioxide (ATO) related manganese arsenite complexes. Acidic media triggered the simultaneous release of ATO, a clinical anticancer drug, and Mn^{2+} cations that enhanced T_1 contrast, hence such probe is promising for monitoring drug delivery in real time. Based on the same principle, the groups of Li and Wang[24] encapsulated MnO NPs inside a hybrid silica nanoshell together with a fluorophore for bimodal imaging. In the presence of acidic media, Mn (II) cations where released and exerted a substantial T_1 contrast enhancement. The probes were validated *in vitro* after incubation with HeLa cells and signal intensity was monitored over time and at increasing concentrations of the probe. A related strategy was pursued by the use of mesoporous manganese silicate coated silica NPs.[25] The manganese silicate shell provided a source of Mn (II) cations at pH values below 7 which were active in MRI. In addition they used the pores to allocate doxorubicin (DOX) so that it would be released as the electrostatic interactions between DOX and pores surface were affected by acidic pH in a combined drug delivery/imaging system. The authors successfully probed their NPs in a tumour model *in vivo* where increased T_1 contrast was clearly observed within the tumour.

In addition to manganese based probes, gadolinium based ones are also employed as pH sensors in MRI. As described in some examples in the previous section, the activation of the

probe is frequently achieved by controlling the accessibility of gadolinium to bind water molecules. Different gadolinium probes were encapsulated in polymeric matrixes[29-32] or dendrimers[28] which changed morphology (either shrank or swelled)[29-31], hydrolysed[30] or protonated[28] in acidic pH. This led to substantial changes in relaxivity values of the probes as a consequence of pH and in some cases also to probe accumulation due to size change.[28-32] In connection with this, Yang et al. encapsulated iron oxide NPs within micelles that disassembled at pH values below 6.8. The micelle rupture and iron oxide NPs release was accompanied by a T_2 contrast enhancement at acidic sites, which was successfully demonstrated in brain ischemic areas in a rat model.[33]

2.3. Redox-responsive ^{1}H MRI probes.

Reducing environments are often encountered in tumour cells due to increased levels of glutathione (GSH).[50] Some probes take advantage of this feature as a trigger and produce or increase their signal in MRI.[10, 11] As in the case of pH, many manganese probes are used since their Mn (III) or Mn (IV) complexes or salts are stable, available and they easily reduce to Mn (II), which is far better as T_1 contrast agent than Mn (III) or Mn (IV).[37, 38] The production of Mn (II) is frequently aided by the low pH also present in cancer cells together with GSH, hence some of the pH-triggered manganese probes are considered as both pH and redox-triggered contrast agents.[25, 35] Several groups used MnO_2 nanosheets that were able to adsorb drugs or biomolecules on their surface and released them together with Mn (II) cations under reducing conditions, causing MRI contrast enhancement, and have been applied to *in vitro* and *in vivo* imaging of cancer.[35, 36] Kim et al.[34] designed a smart T_1/T_2 dual mode redox-responsive probe by coating iron oxide NPs with a shell of Mn_3O_4. In the OFF state the relaxivity of the probe was very low, but in the presence of GSH the shell disintegrated into Mn (II) ions and exposed the iron oxide NPs, increasing both r_1 and r_2 (Figure 3). The feasibility of such dual imaging

approach in reducing environments present in tumours was evaluated in cells and *in vivo* in an animal model. Based on the same principle, the r_1 fluctuations when shifting from Cu(II) to Cu(I) and *vice versa* have been postulated as potential redox activatable probes although the T_1 contrast ability of copper is very reduced compared with gadolinium or manganese.[39]

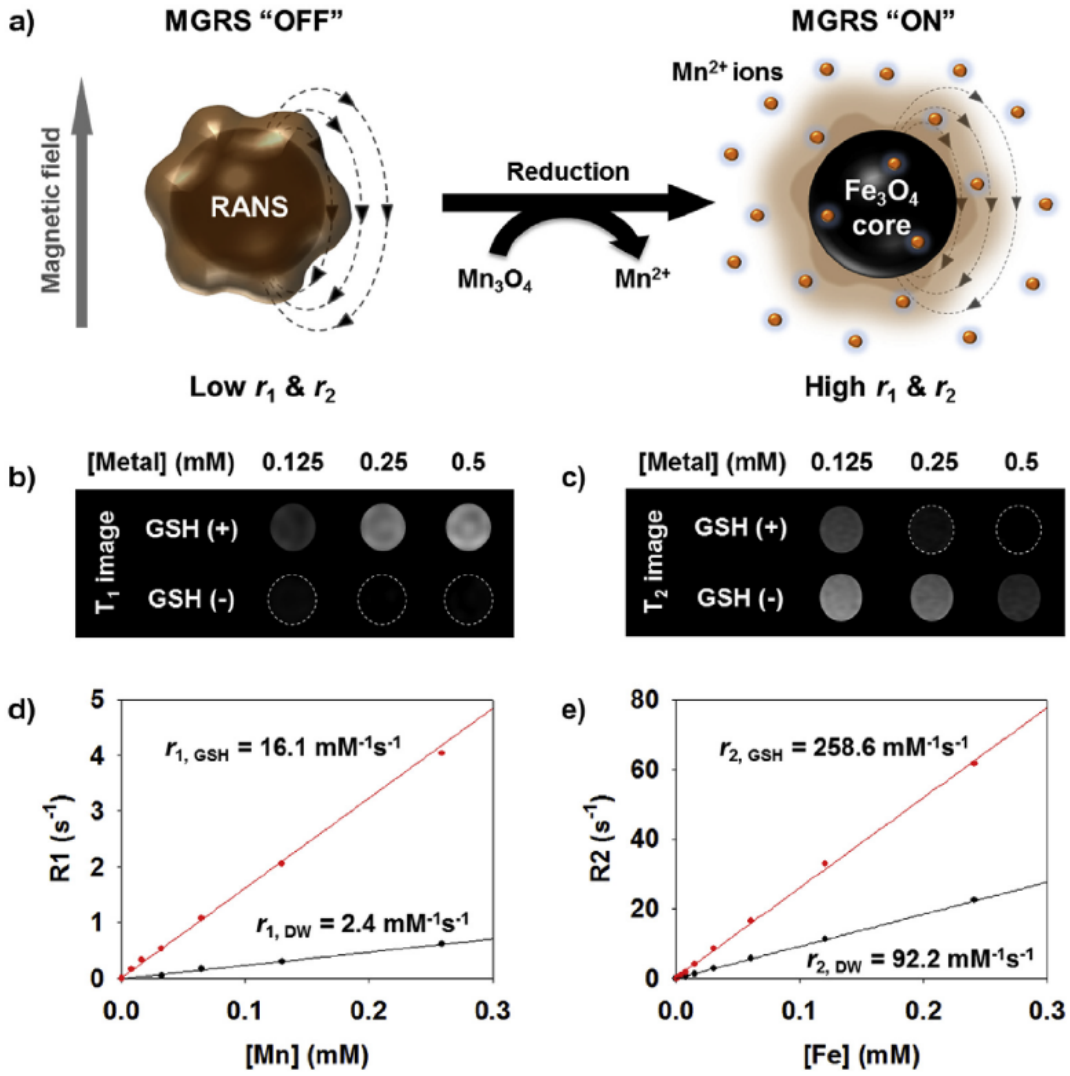

Figure 3. A) Proposed mechanism of magnetic relaxation switch for activatable MR imaging in reducing environments. B) T1 and C) T2-weighted image of the probe after treatment with GSH and non-treatment. D, E) Relaxivity plot of with respect to Mn or Fe concentration. Reprinted from Biomaterials, 101, M.-H. Kim, H.-Y. Son, G.-Y. Kim, K. Park, Y.-M. Huh, S. Haam, Redoxable heteronanocrystals functioning magnetic relaxation switch for activatable T_1 and T_2 dual-mode

magnetic resonance imaging, 121-130, Copyright (2016), with permission from Elsevier (Ref. 34).

For Gd probes other strategies are pursued. For example, Muñoz Úbeda et al.[40] reported the binding of a Gd chelate to silica microparticles through a short and redoxable linkage consisting of a disulfide bond. When such linker was cleaved in the presence of GSH, the Gd chelate separated from the particles and the r_1 increased substantially due to the increase in the tumbling rate. Interestingly, the authors proposed the use of such probe for the detection of redox environments in artificial extracellular matrix to determine whether cell grafts were metabolically active or hypoxic, by MRI. Other related example comprised the trapping of Gd (III) inside polymeric NPs with redox labile bonds that after being reduced exposed Gd (III) to water molecules increasing the r_1 to really high values, up to approximately 52 $mM^{-1}s^{-1}$.[42] The group of Rao used their previously mentioned strategy in section 2.1 of macrocyclisation to *in situ* build Gd-labelled NPs induced by the presence of GSH. The so-obtained NPs displayed roughly a 60% increase in r_1 relaxivity values.[41]

2.4. Ion-responsive ^{1}H MRI probes.

The vast majority of activatable probes for ion detection are focused on the detection of Ca (II) due to its relevance in the central nervous system (CNS), where it acts as a transducer of electrical activity and hence it is of interest to track neuronal activity. In most examples small molecules were used consisting of Gd chelates further modified to accommodate Ca (II) cations through chelation. Such Ca (II) complexation in the vicinity of Gd complexes induced an increase of r_1 relaxivity. In the OFF state (absence of calcium) Ca-binding ligands hampered the accessibility of Gd to water. However, when Ca was present, the water accessibility was

restored and the probe turned ON (Figure 4).[43-45] Probes based on this mechanism have been used to monitor intracellular Ca (II) in hippocampal neuronal cells[43] and astrocytes.[44]

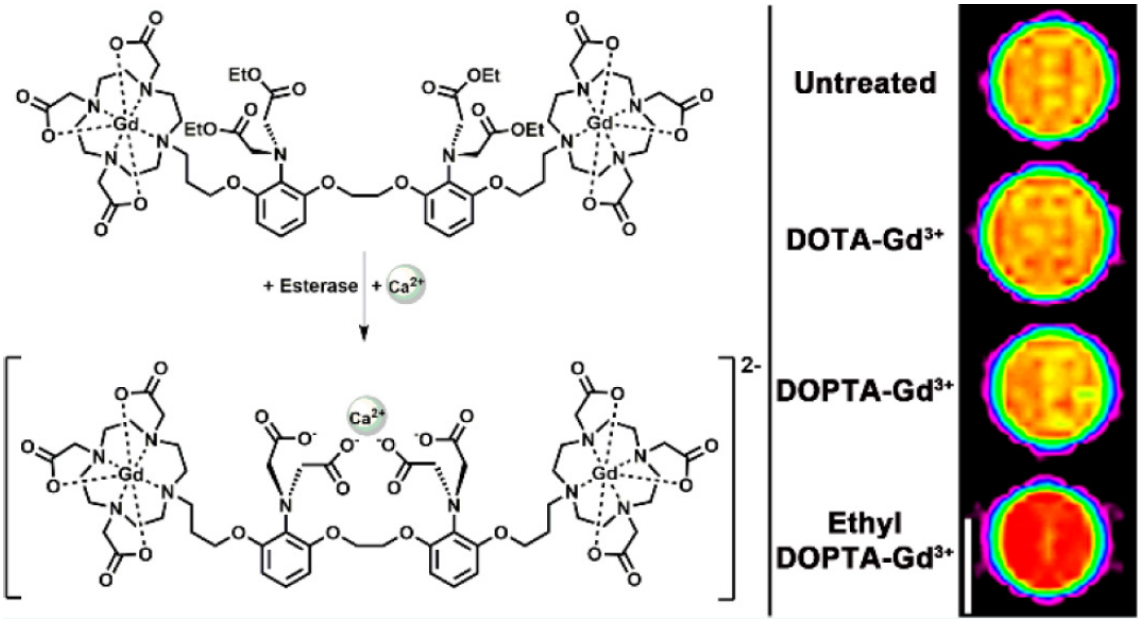

Figure 4. On the left, probe structure and calcium chelation. On the right, image intensity color map of T1-weighted MR images of cells incubated with several Gd probes and media alone. Reprinted with permission from Bioconjugate Chemistry, 27, K.W. MacRenaris, Z. Ma, R.L. Krueger, C.E. Carney, T.J. Meade, Cell-Permeable Esterase-Activated Ca(II)-Sensitive MRI Contrast Agent, 465–473. Copyright (2016) American Chemical Society (Ref. 43).

The same OFF/ON strategy was used but using a Gd chelate modified for Ca (II) complexation linked to a dendrimer. In this case the authors proposed a ratiometric method based on measuring variations in the R_1/R_2 ratio in the absence and presence of Ca (II). This ratio change was rapidly recorded by balanced steady-state free precession (bSSFP) imaging protocol and this approach was proposed as a mean to image dynamic processes with very fast kinetics.[46] Apart from calcium, copper is another biologically relevant cation. Modifications in Cu homeostasis seem to be related to neurodegenerative pathologies. Indeed, some genetic

disorders, such as Menkes disease, are a consequence of mutations in copper handling proteins. Que et al.[47] designed a Gd-DO3A modified with a thioether chelating moiety able to link selectively Cu(I) in the presence of other cations, leading to a clear increase in r_1 value. Such probe was successfully tested *in vitro* in a Menkes disease model cell line that was exposed to copper.

2.5. Other examples of responsive ^{1}H MRI probes.

As we have seen so far, the most common triggers to stimulate activatable probes in MRI are enzymes, pH, reducing environments and certain cations. Although much less frequent in the literature, other phenomena could also turn ON the signal of specifically designed probes, such as for instance the presence of small molecules like cocaine. Interestingly, although the aim of most of enzyme responsive probes is to study the enzyme activity as a cancer biomarker, the research group of Lu[48] proposed the use of phosphatidylcholine 2-acetylhydrolase (PLA_2) enzyme as a tool to connect small molecule detection with MRI signal production. They designed smart liposomes loaded with gadopentetic acid (Gd-DTPA) which was released due to liposome degradation by PLA_2 as a result of the presence of cocaine. Firstly, magnetic beads were functionalised by hybridisation with DNA aptamers conjugated to PLA_2. The presence of cocaine led to a weakening in the DNA hybridisation due to cocaine-aptamer recognition and triggered the release of DNA-PLA_2 conjugates which then degraded the liposomes and released the MRI probe. Such release as a consequence of cocaine triggered PLA_2 activity was monitored by the increase of T_1 contrast as cocaine concentration increased in T_1-weighted images. The authors also showed that they could load the liposome not only with Gd-DTPA, but also with uranin fluorophores to produce a multimodal probe with application in MRI and optical imaging. The system could in principle be extended to other small molecules apart from cocaine by selecting the right DNA aptamers for each analyte.

3. Activatable probes for ^{19}F MRI probes.

Fluorine 19 based MRI (^{19}F MRI) has recently attracted increasing attention due to its interesting features which complement ^{1}H MRI. In terms of sensitivity, the ^{19}F isotope has a 100% of natural abundance and its signal to noise ratio (SNR) in magnetic resonance is comparable to that of ^{1}H. Nonetheless, the most interesting advantage of ^{19}F over ^{1}H is the negligible endogenous ^{19}F MRI signal in the body, for which any detectable signal can only come from an exogenous probe. This lack of background in ^{19}F MRI images translates into the fact that the probe is imaged directly, allowing for the absolute quantification of the signal that is directly proportional to the probe concentration. Since there is no detectable background signal, fluorine based probes are ideal candidates for the design of OFF/ON systems, in which the signal is temporarily shut down and subsequently triggered by some external stimuli. There are several strategies to quench or turn OFF the fluorine signal. The most common strategies are either by proximity of a paramagnetic metal, or by entrapping the probe in a more rigid environment (mobility restriction). The separation from the paramagnetic metal or the release from the mobility constrain would trigger the signal in each case, turning ON the probe. However, in order to obtain images with similar quality to those of conventional MRI based on very abundant water molecules, we need a high amount of fluorine. For this reason, the major challenge when designing fluorine based probes is to find a balance between high fluorine loading to obtain the highest ^{19}F MRI signal possible and water solubility of the probe by overcoming fluorine intrinsic hydrophobicity. Fluorine based activatable probes have been barely reviewed,[13] hence we will include references from the last decade and not only from the last two years. As before, we will discuss the probes with respect to the trigger that activates them. A table summary is included with all the examples collecting the trigger, its consequence, the effect observed in MRI (or NMR in some preliminary studies) and if they have been tested in solution (proof of concept), cells or *in vivo* (Table 2).

Table 2. Summary of ^{19}F MRI activatable probes.

	Probe	Enzyme and consequence	Effect observed	Application	Ref.
Enzyme-responsive probes	Gd-peptide-^{19}F	Caspase 3/7 directed peptide degradation	PRE effect cancellation. ^{19}F MRI signal ON.	Caspase 3/7 activity detection. Proof of concept in solution	51
	^{19}F-NP assembly	Caspase 3/7 induced disassembly	^{19}F MRI signal ON.	Caspase 3/7 activity detection *in vivo*	52
	^{19}F-NP assembly	Legumain induced disassembly	^{19}F MRI signal ON.	Legumain activity detection *in vivo*	53
	^{19}F-dendron assembly	PLE induced dendron diassembly	^{19}F MRI signal ON.	Proof of concept in solution	54
	^{19}F-micelles	PLE induced micelle disassembly	^{19}F MRI signal ON.	Proof of concept in solution	55
	^{19}F-hydrogel	ALP controlled assembly and tyrosine kinase directed disassembly	^{19}F MRI signal OFF (ALP) ^{19}F MRI signal ON (Tyrosine kinase)	ALP and tyrosine kinase activities detection *in vitro*	56
	SiO_2 NP – ^{19}F dendrimer	ALP induced dendrimer cleavage	^{19}F MRI signal ON.	ALP activity detection. Proof of concept in solution	57
	^{19}F-assemblies	MMP-2 induced disassembly	^{19}F MRI signal ON.	*In vitro* MMP-2 detection	58
	Gd-peptide-^{19}F	MMP-2 directed peptide degradation	PRE effect cancellation. ^{19}F MRI signal increase.	*In vitro* MMP-2 activity monitoring	59
	Gd-chelate-^{19}F	β-galactosidase directed ligand cleavage	PRE effect cancellation. ^{19}F MRI signal ON.	β-galactosidase activity detection. Proof of concept in solution	60
	^{19}F-β-D-galactopyranoside	β-Galactosidase induced probe degradation	^{19}F NMR chemical shift upon enzyme action	*In vitro* β-Galactosidase and LacZ transgene activity detection	61
	^{19}F-β-D-galactopyranoside	β-Galactosidase	^{19}F NMR chemical shift upon enzyme action	*In vitro* and *in vivo* β-Galactosidase and LacZ transgene activity detection	62
pH-responsive probes	**Probe**	**pH consequence**	**Effect observed**	**Application**	**Ref.**
	^{19}F-micelles	Micelles disassembly at pH < 7	^{19}F MRI signal ON.	Proof of concept in solution	63
	^{19}F@nanogels	Nanogels swelling at pH < 7	^{19}F MRI signal ON.	Proof of concept in solution	64
	^{19}F@mesoporous SiO_2 NPs	^{19}F probe release	^{19}F MRI signal ON.	*In vitro* acidic pH detection	65
	^{19}F-peptide nanostructures	Probe morphological changes	^{19}F MRI signal ON.	Proof of concept in solution	66
redox-responsive probes	**Probe**	**Redox consequence**	**Effect observed**	**Application**	**Ref.**
	^{19}F-NP assembly	GSH induced assembly	^{19}F MRI signal OFF.	*In vivo* cancer diagnosis.	52, 53
	^{19}F- Fe (III) chelate	Reduction of Fe (III) to Fe (II)	PRE effect cancellation. ^{19}F MRI signal ON.	Proof of concept in solution	67
	^{19}F- Cu (II) chelate	Hypoxia induced reduction of Cu (II) to Cu (I)	PRE effect cancellation. ^{19}F MRI signal ON.	Proof of concept in solution	68
	^{19}F@SiO_2 -Gd-chelate	Gd chelate release	PRE effect cancellation. ^{19}F MRI signal ON.	Proof of concept in solution	69
Other examples	**Probe**	**Trigger and consequence**	**Effect observed**	**Application**	**Ref.**
	^{19}F-chelation ligand	Zn (II) or Fe(II) chelation	Chemical shift variations in CEST	Simultaneous ion detection. Proof of concept in solution	70
	^{19}F-polymer	Na^{1+} induced conformational changes	Decrease in T_2 at increasing NaCl concentration	*In vitro* detection of cancer cells	71
	^{19}F- assembly	Protein recognition leading to probe disassembly	^{19}F MRI signal ON.	*In vitro* protein detection	72

Abbreviations: PLE: porcine liver esterase; ALP: alkaline phosphatase; PRE: paramagnetic relaxation enhancement. @ = encapsulated in.

3.1. Enzyme-responsive ^{19}F MRI probes.

As with ^{1}H MRI activatable probes, enzymatic activity is a major focus of research in the field of ^{19}F MRI probes, because of their potential role as disease biomarkers, more particularly as cancer biomarkers. As explained at the beginning of this review (Section 2.1), detection of caspase 3/7 activity is regarded as an indication of cellular apoptosis and it is of interest in the evaluation of tumour therapy. The research group of Kikuchi[51] designed a probe that connected a Gd chelate with a fluorinated compound through a short peptide cleavable by caspase 3/7 (DVED). Initially the ^{19}F signal was turned OFF by the paramagnetic relaxation enhancement effect (PRE), in which the presence of a paramagnetic compound in the vicinity of fluorine produced a shortening of its T_2 value and hence a substantial attenuation of MRI signal was observed. In the presence of caspase 3/7, the peptide was cleaved and the Gd chelate separated from fluorine turning ON the ^{19}F MRI signal. Yue et al.[59] also took advantage in a similar manner of the PRE effect of Gd over fluorine by linking a Gd chelate with a fluorine label through a peptide sensitive to MMP-2 enzyme. The authors observed the signal increase and sharpening over time as they exposed the probe to the enzyme. Likewise, Keliris et al.[60] used a related approach in which the action of β-galactosidase on their probe produced the separation of a fluorine probe from a Gd chelate cancelling its PRE effect.

Nonetheless, the assembly/disassembly approach is one of the most frequently used to quench/activate ^{19}F MRI signal, because mobility restriction of the fluorine atoms is easy to achieve by encapsulation or trapping techniques and it leads to ^{19}F signal broadening and hence MRI signal attenuation. Yuan[52] et al. designed a smart probe for imaging caspase 3/7 activity *in vivo*. They prepared a fluorine probe, based also on the DVED peptide, which assembled into NPs in the presence of reducing GSH, which is abundant in tumour cells. When the fluorine probe was forming NPs, they had no detectable ^{19}F MRI signal so they were in the OFF state. Then, in the presence of caspase 3/7, NPs disassembled and the signal turned ON

(Figure 5). The authors tested it on a zebrafish model using a control probe that was able to assemble into NPs but it was not cleaved by caspase 3/7, hence it remained in the OFF state. By selectively changing the peptide in the probe, the authors used the same strategy of glutathione induced assembly and enzymatic disassembly to detect legumain enzyme in zebrafish.[53] These probes served not only to study the so-targeted enzyme but also the presence of GSH.

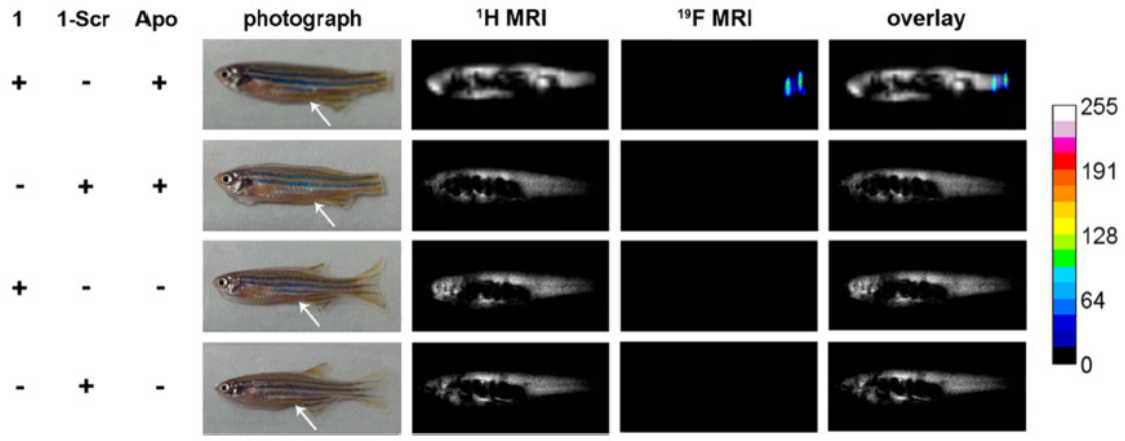

Figure 5. Topmost row: Fluorinated probe (**1**) injected into the enterocoelia of zebrafish 3 h after tail amputation. Top middle row: Control probe (**1-Scr**) injected into the enterocoelia of zebrafish 3 h after tail amputation. Bottom middle row: **1** injected into the enterocoelia of a healthy zebrafish. Bottom-most row: **1-Scr** injected into the enterocoelia of a healthy zebrafish. Fluorine MRI signal was only detected in the zebrafish after tail amputation injected with fluorinated probe **1**. Reprinted with permission from ACS Nano, 9, Y. Yuan, H. Sun, S. Ge, M. Wang, H. Zhao, L. Wang, L. An, J. Zhang, H. Zhang, B. Hu, J. Wang, G. Liang, Controlled Intracellular Self-Assembly and Disassembly of ^{19}F Nanoparticles for MR Imaging of Caspase 3/7 in Zebrafish, 761-768. Copyright (2015) American Chemical Society (Ref. 52).

The groups of Liu and Liang[56] designed a fluorinated hydrogel precursor that could detect the presence of two enzymes. On the one hand, alkaline phosphatase (ALP) directed the assembly

of the fluorinated precursor into a hydrogel with non-detectable ^{19}F MRI signal and on the other hand, tyrosine kinase controlled the hydrogel disassembly and the subsequent turning ON of the ^{19}F MRI signal. Some other examples of assembly/disassembly approach for enzymatic activity detection included porcine liver esterase (PLE) directed rupture of fluorinated dendrons,[54, 55] alkaline phosphatase induced release of perfluorinated dendrimers[57] or MMP-2 degradation of fluorine modified peptide aggregates.[58]

Other approaches involved the use of nuclear magnetic resonance (NMR) to detect variations in the chemical shift of fluorine atoms upon enzymatic activity on the fluorinated probe. These kinds of examples are scarce and have only been applied to the detection of β-galactosidase and LacZ transgene activity.[61, 62]

3.2. pH-responsive ^{19}F MRI probes.

In the case of pH-responsive probes, one common approach takes advantage of the protonation of different types of matrixes by selectively choosing the pK_a of the matrix components so that the protonation takes place in the approximate pH range of 5 to 7, which is biologically interesting mostly as a cancer biomarker. In this context, the research group of Gao[63] reported a smart micelle able to detect specific pH transitions at pH values of 6.5, 5.5 and 4.5. The authors prepared three kinds of block-copolymers each of them with a different fluorine probe and amine moiety with pK_a values ranging from 7 to 5, so that the protonation of such amine groups would take place at different pH values. When the micelles were assembled the fluorine signal in MRI was OFF. However, when the samples were subjected to specific pH values just below the pK_a of their amine moieties, the micelles disassembled and the fluorine signal turned ON. In addition, they used a colour barcode system to read the pH (Figure 6).

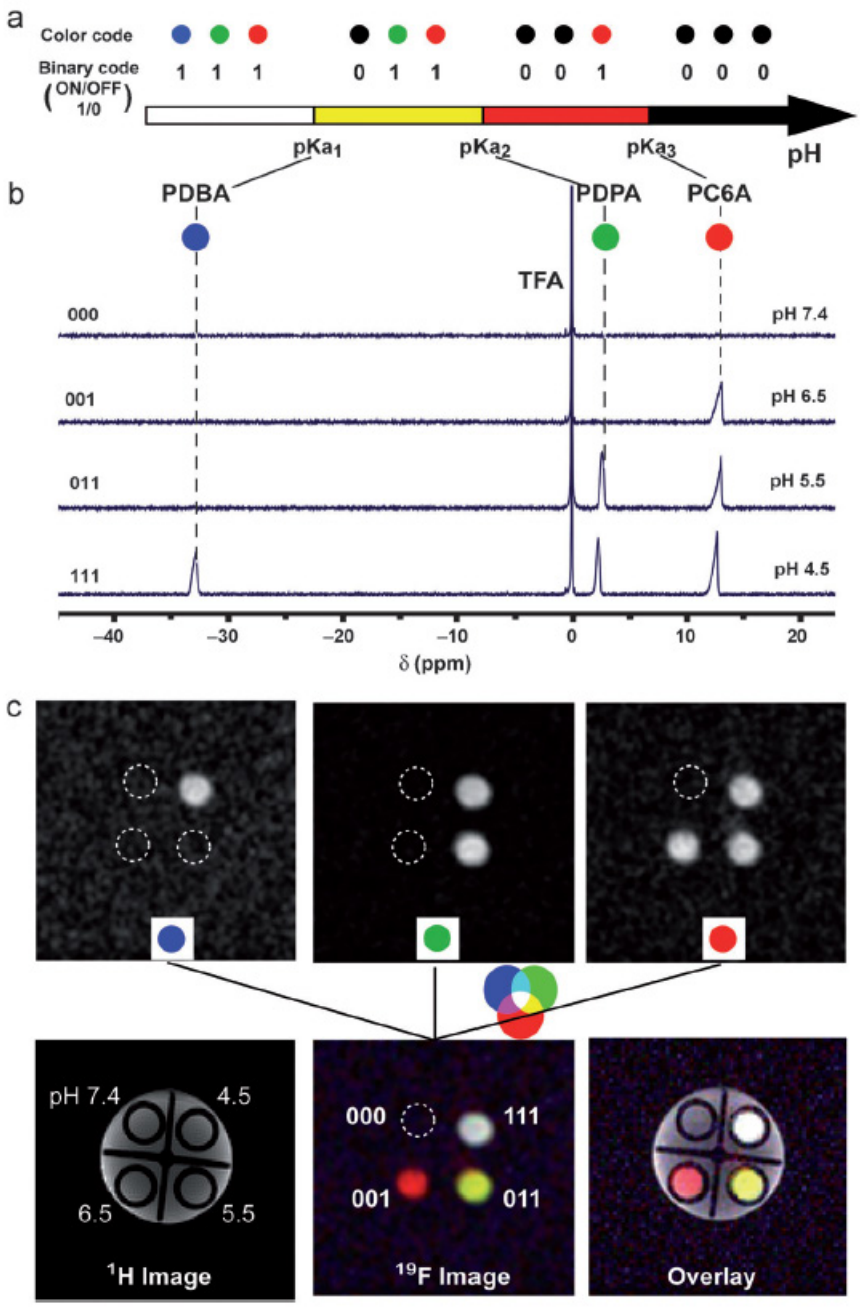

Figure 6. A) Schematic illustration of the colour barcode concept for direct readout of pH values B) ^{19}F spectra of a mixture of three fluorinated nanoprobes at different pH values. c) ^{19}F MR imaging of the same nanoprobe mixture in solutions with different pH values and using the barcode map. Reprinted with permission from Angewandte Chemie International Edition, 52, X. Huang, G. Huang, S. Zhang, K. Sagiyama, O. Togao, X. Ma, Y. Wang, Y. Li, T. C. Soesbe, B. D. Sumer, M. Takahashi, A. D. Sherry, J. Gao, Multi-Chromatic pH-Activatable ^{19}F-MRI Nanoprobes

with Binary ON/OFF pH Transitions and Chemical-Shift Barcodes, 8074 - 8078. Copyright (2013) John Wiley and Sons (Ref. 63).

Likewise, a similar strategy was employed by the use of PEGylated nanogels with a hydrophobic fluorinated probe. Under basic conditions the gel was non-hydrated and the fluorine lacked mobility so its signal was OFF. However, pH values below 7 led to nanogel hydration and swelling which implied an increase of mobility of the fluorinated core and the signal turned ON. Such probe was validated by ^{19}F NMR.[64] Related to these examples, other authors took advantage of the pK_a of their probes to produce substantial morphological changes at acidic pH that had an impact in fluorine signal. Preslar et al.[66] reported on supramolecular nanostructures comprising amphiphilic fluorinated peptides. At pH values higher than 7 the fluorinated nanostructures arranged forming ribbons with a dense packing and no fluorine signal in MRI. However, under acidic conditions, they arranged in the form of cylinders and the ^{19}F MRI signal turned on. The authors attributed the signal changes to increased mobility of the fluorine probe in the cylindrical nanostructures.

Chen et al.[65] took a different approach and prepared a novel, nanosized and pH-triggered probe based on encapsulation of a fluorinated compound within the pores of mesoporous silica NPs capped with gold NPs. Such gold NPs were linked to the surface of the pores by a hydrazone covalent bond which is a pH-sensitive bond. At pH below 6 the hydrazone linkage was hydrolysed and the fluorine probe released with concomitant ^{19}F MRI signal activation. The authors also labelled the system with a fluorophore for dual fluorescence/^{19}F MRI imaging (Figure 7).

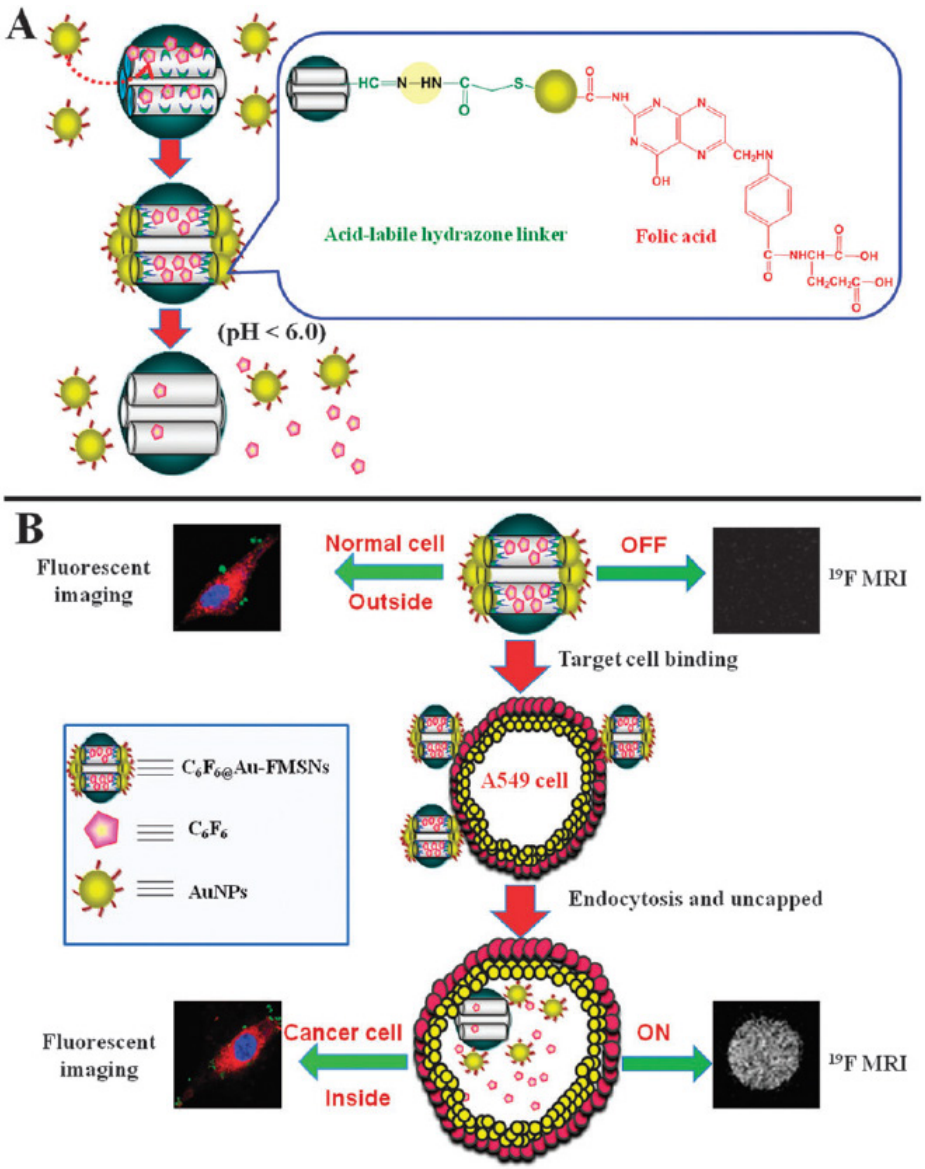

Figure 7. A) The synthesis of the pH-sensitive probe. B) The acidic pH-triggered release of the ^{19}F contrast agent to the cytosol via the selective removal of the gold NP cap in the acidic intracellular compartments of cancer cells. Reproduced from Ref. 65 with permission from The Royal Society of Chemistry.

3.3. Redox-responsive ^{19}F MRI probes.

There are few examples of redox responsive ^{19}F MRI probes and most of them take advantage of the PRE effect induced by paramagnetic metals in the neighbourhood of ^{19}F nuclei. In one

example, the authors used the Fe(III)/Fe(II) pair as a reversible switch to turn OFF/ON the fluorine signal. They prepared a cubic octameric polyhedral oligomeric silsesquioxanes functionalised with ferrocene as the redoxable switch combined with a trifluoromethyl moiety as the fluorine probe. When the iron source was in the form of Fe (II) the signal was ON, but when oxidised to Fe (III) with ammonium persulfate (APS) the signal was OFF. Interestingly, it was possible to reduce the system back to Fe (II) with a mild reductant such as ascorbic acid turning the signal ON again.[67] An analogous approach based on the PRE effect but using the Cu(II)/Cu(I) pair has been recently reported. The authors designed a copper (II) chelate with a fluorinated side chain. The fluorine atoms, being close to Cu (II) were inactive in ^{19}F NMR. However, the fluorine signal was activated when Cu (II) was reduced to Cu (I) in hypoxic cells.[68] In a different approach, Nakamura et al.[69] encapsulated a fluorinated probe inside silica NPs, which were further decorated with a Gd chelate linked through a redox sensitive disulfide bond. While the Gd chelate was linked to the surface of silica NPs, ^{19}F MRI signal was OFF. In a reducing environment, the disulfide bond was cleaved and the Gd chelate separated from the fluorine probe allowing it to be detected in MRI (Figure 8). In this section it should also be mentioned the work of Yuan et al. already discussed in section 3.1, where they used the presence of reducing GSH to assemble NPs that led to the quenching of ^{19}F MRI signal.[52, 53]

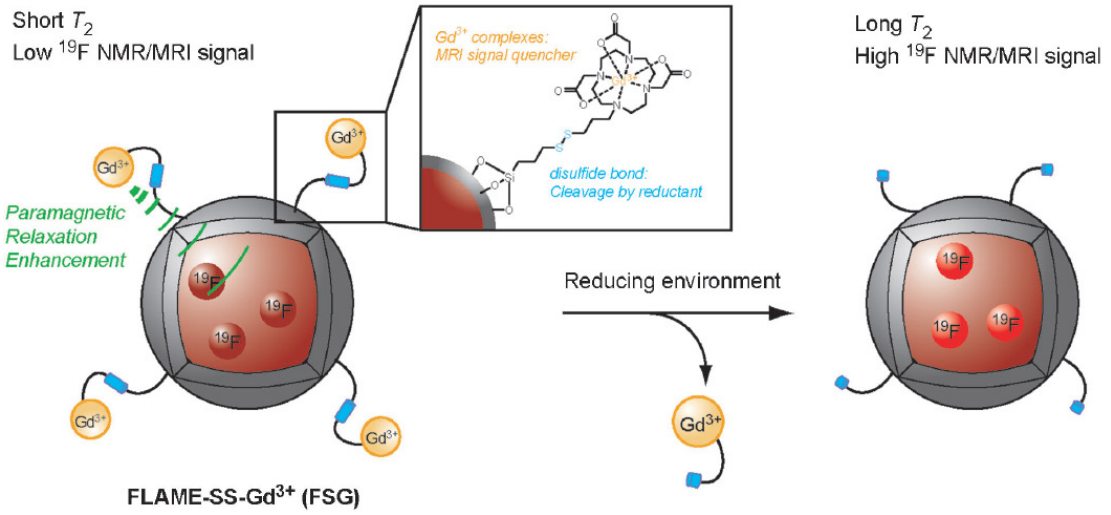

Figure 8. Design of activatable Gd decorated cage, with encapsulated fluorine probe, and release mechanism in a reducing environment. Reprinted with permission from Angewandte Chemie International Edition, 54, T. Nakamura, H. Matsushita, F. Sugihara, Y. Yoshioka, S. Mizukami, K. Kikuchi, Activatable ^{19}F MRI Nanoparticle Probes for the Detection of Reducing Environments, 1007 - 1010. Copyright (2015) John Wiley and Sons (Ref. 69).

3.4. Other examples of responsive ^{19}F MRI probes.

The research group of Hamachi[72] proposed a probe to detect proteins, both of enzymatic and non-enzymatic nature. The authors built a fluorinated probe linked to a known ligand of the chosen target protein. The probe was silent when assembled but the fluorine signal was triggered in the presence of the target protein through a protein-probe binding-mediated disassembly which turned ON the signal with a sharp transition from the OFF to the ON state. In their case they selected human carbonic anhydrase I (hCAI) and used a benzenesulfonamide moiety as the specific ligand for hCAI. Hence, when the ligand got in contact with hCAI, it bound and provoked the probe disassembly and the successful turn ON of the ^{19}F signal. By modifying the probe accordingly with the necessary ligands they extended their methodology to the detection of other proteins such as trypsin or avidin.

Zhang et al.[71] have recently reported on an ion-responsive probe for the detection of cancer cells. They used high resolution ^{19}F NMR and spin-spin relaxation time measurements to study conformational changes of fluorinated polymers in the presence of different ionic environments, such as those present in different cell lines. Those changes could be correlated with the differences in ionic environment depending on the studied cell line. In particular they observed significantly shorter T_2 times in cancer cells as compared with healthy cells. In another example, the group of Bulte[70] took advantage of the chemical shift offset in CEST of a

tetrafluorinated compound (TF-BAPTA) when acting as a chelator of different biologically relevant cations, more particularly Zn^{2+} and Fe^{2+} and created CEST maps to detect those ions.

4. Conclusions.

According to the number of publications in the last years, the development of smart probes to aid diagnosis by MRI is a field of increasing interest. The possibility to visualize within organs and in real time dynamic processes, such as enzymatic activity, complements the already existing possibilities of MRI as a functional imaging tool, apart from delivering anatomical information. In this regard, the field of responsive probes for ^{1}H MRI is far more advanced than that of ^{19}F MRI. This is probably due to the longer tradition in T_1 and T_2 contrast design research, their clinical applicability and the plethora of probes available. However, there is yet room for research since most of the probes are devoted to the study of cancer, while other pathologies are less explored although they also have a high incidence, such as cardiovascular diseases. In addition, most of the ^{1}H MRI based probes are not pure OFF/ON contrast agents since they usually provoke an increase of an already existing albeit low signal, hence detection of signal variations when differences are small might be tricky. On the contrary, the field of activatable probes for ^{19}F MRI is comparatively underexplored. This is likely due to the higher complexity of fluorinated probe design since a high amount of fluorine is required, which is highly hydrophobic, but yet the water solubility of the probe must be maintained. However, fluorinated probes are ideal candidates for OFF/ON systems because there is no background signal. Hence, the probe detection is unequivocal, it can be quantified directly, and it is relatively easy to modulate the ^{19}F MRI signal. Unfortunately, very few of these fluorine activatable probes have been tested *in vivo* so far, most likely due to sensitivity problems because of insufficient fluorine concentration.

Acknowledgements

MC acknowledges Ikerbasque for a Research Fellow position and funding from MINECO through the call RETOS (CTQ2015-68413-R to MC).

References.

1. Y. Cui, W. Du and G. Liang, *Chemnanomat*, 2016, **2**, 344-353.
2. J. Li, F. Cheng, H. Huang, L. Li and J.-J. Zhu, *Chemical Society Reviews*, 2015, **44**, 7855-7880.
3. S. M. J. van Duijnhoven, M. S. Robillard, S. Langereis and H. Grull, *Contrast Media & Molecular Imaging*, 2015, **10**, 282-308.
4. T. Anani, P. Panizzi and A. E. David, *Nanomedicine*, 2016, **11**, 2007-2022.
5. D. V. Hingorani, A. S. Bernstein and M. D. Pagel, *Contrast Media & Molecular Imaging*, 2015, **10**, 245-265.
6. D. V. Hingorani, B. Yoo, A. S. Bernstein and M. D. Pagel, *Chemistry-a European Journal*, 2014, **20**, 9840-9850.
7. G. Angelovski, *Angewandte Chemie-International Edition*, 2016, **55**, 7038-7046.
8. G.-L. Davies, I. Kramberger and J. J. Davis, *Chemical Communications*, 2013, **49**, 9704-9721.
9. C. Tu and A. Y. Louie, *Nmr in Biomedicine*, 2013, **26**, 781-787.
10. Q. N. Do, J. S. Ratnakar, Z. Kovacs and A. D. Sherry, *Chemmedchem*, 2014, **9**, 1116-1129.
11. P. B. Tsitovich, P. J. Burns, A. M. McKay and J. R. Morrow, *Journal of Inorganic Biochemistry*, 2014, **133**, 143-154.
12. C. Shen and E. J. New, *Current Opinion in Chemical Biology*, 2013, **17**, 158-166.
13. K. Kikuchi, *Bulletin of the Chemical Society of Japan*, 2015, **88**, 518-521.
14. R. A. Moats, S. E. Fraser and T. J. Meade, *Angewandte Chemie-International Edition in English*, 1997, **36**, 726-728.
15. Z. Cheng and A. Tsourkas, *Scientific Reports*, 2014, **4**.
16. H. Nejadnik, D. Ye, O. D. Lenkov, J. S. Donig, J. E. Martin, R. Castillo, N. Derugin, B. Sennino, J. Rao and H. Daldrup-Link, *Acs Nano*, 2015, **9**, 1150-1160.
17. D. Ye, A. J. Shuhendler, P. Pandit, K. D. Brewer, S. S. Tee, L. Cui, G. Tikhomirov, B. Rutt and J. Rao, *Chemical Science*, 2014, **5**, 3845-3852.
18. G. S. Loving and P. Caravan, *Angewandte Chemie-International Edition*, 2014, **53**, 1140-1143.
19. G. G. Westmeyer, Y. Emer, J. Lintelmann and A. Jasanoff, *Chemistry & Biology*, 2014, **21**, 422-429.
20. C. Ansari, G. A. Tikhomirov, S. H. Hong, R. A. Falconer, P. M. Loadman, J. H. Gill, R. Castaneda, F. K. Hazard, L. Tong, O. D. Lenkov, D. W. Felsher, J. Rao and H. E. Daldrup-Link, *Small*, 2014, **10**, 566-575.
21. J. He, C. S. Bonnet, S. V. Eliseeva, S. Lacerda, T. Chauvin, P. Retailleau, F. Szeremeta, B. Badet, S. Petoud, E. Toth and P. Durand, *Journal of the American Chemical Society*, 2016, **138**, 2913-2916.
22. B. Yoo, V. R. Sheth, C. M. Howison, M. J. K. Douglas, C. T. Pineda, E. A. Maine, A. F. Baker and M. D. Pagel, *Magnetic Resonance in Medicine*, 2014, **71**, 1221-1230.
23. M. Haris, A. Singh, I. Mohammed, R. Ittyerah, K. Nath, R. P. R. Nanga, C. Debrosse, F. Kogan, K. Cai, H. Poptani, D. Reddy, H. Hariharan and R. Reddy, *Scientific Reports*, 2014, **4**.

24. B. Y. W. Hsu, M. Ng, A. Tan, J. Connell, T. Roberts, M. Lythgoe, Y. Zhang, S. Y. Wong, K. Bhakoo, A. M. Seifalian, X. Li and J. Wang, *Advanced Healthcare Materials*, 2016, **5**, 721-729.
25. X. Li, W. Zhao, X. Liu, K. Chen, S. Zhu, P. Shi, Y. Chen and J. Shi, *Acta Biomaterialia*, 2016, **30**, 378-387.
26. P. Mi, D. Kokuryo, H. Cabral, H. Wu, Y. Terada, T. Saga, I. Aoki, N. Nishiyama and K. Kataoka, *Nature Nanotechnology*, 2016, **11**, 724-+.
27. Z. Zhao, X. Wang, Z. Zhang, H. Zhang, H. Liu, X. Zhu, H. Li, X. Chi, Z. Yin and J. Gao, *ACS Nano*, 2015, **9**, 2749-2759.
28. M. P. I. Bhuiyan, M. P. Aryal, B. Janic, K. Karki, N. R. S. Varma, J. R. Ewing, A. S. Arbab and M. M. Ali, *Contrast Media & Molecular Imaging*, 2015, **10**, 481-486.
29. S. Okada, S. Mizukami, T. Sakata, Y. Matsumura, Y. Yoshioka and K. Kikuchi, *Advanced Materials*, 2014, **26**, 2989-2992.
30. M. L. Viger, J. Sankaranarayanan, C. d. G. Lux, M. Chan and A. Almutairi, *Journal of the American Chemical Society*, 2013, **135**, 7847-7850.
31. R. Liu, S. Liang, C. Jiang, L. Zhang, T. Yuan, P. Li, Z. Xu, H. Xu and P. K. Chu, *Journal of Materials Chemistry B*, 2016, **4**, 1100-1107.
32. L. Zhu, Y. Yang, K. Farquhar, J. Wang, C. Tian, J. Ranville and S. G. Boyes, *Acs Applied Materials & Interfaces*, 2016, **8**, 5040-5050.
33. H. Y. Yang, M.-S. Jang, G. H. Gao, J. H. Lee and D. S. Lee, *Nanoscale*, 2016, **8**, 12588-12598.
34. M.-H. Kim, H.-Y. Son, G.-Y. Kim, K. Park, Y.-M. Huh and S. Haam, *Biomaterials*, 2016, **101**, 121-130.
35. Y. Hao, L. Wang, B. Zhang, D. Li, D. Meng, J. Shi, H. Zhang, Z. Zhang and Y. Zhang, *International journal of nanomedicine*, 2016, **11**, 1759-1778.
36. Z. Zhao, H. Fan, G. Zhou, H. Bai, H. Liang, R. Wang, X. Zhang and W. Tan, *Journal of the American Chemical Society*, 2014, **136**, 11220-11223.
37. E. M. Gale, S. Mukherjee, C. Liu, G. S. Loving and P. Caravan, *Inorganic Chemistry*, 2014, **53**, 10748-10761.
38. G. S. Loving, S. Mukherjee and P. Caravan, *Journal of the American Chemical Society*, 2013, **135**, 4620-4623.
39. L. Dunbar, R. J. Sowden, K. D. Trotter, M. K. Taylor, D. Smith, A. R. Kennedy, J. Reglinski and C. M. Spickett, *Biometals*, 2015, **28**, 903-912.
40. M. M. Ubeda, F. Carniato, V. Catanzaro, S. Padovan, C. Grange, S. Porta, C. Carrera, L. Tei and G. Digilio, *Chemistry-a European Journal*, 2016, **22**, 7716-7720.
41. D. Ye, P. Pandit, P. Kempen, J. Lin, L. Xiong, R. Sinclair, B. Rutt and J. Rao, *Bioconjugate Chemistry*, 2014, **25**, 1526-1536.
42. S. J. Sigg, F. Santini, A. Najer, P. U. Richard, W. P. Meier and C. G. Palivan, *Chemical Communications*, 2016, **52**, 9937-9940.
43. K. W. MacRenaris, Z. Ma, R. L. Krueger, C. E. Carney and T. J. Meade, *Bioconjugate Chemistry*, 2016, **27**, 465-473.
44. G. Angelovski, S. Gottschalk, M. Milosevic, J. Engelmann, G. E. Hagberg, P. Kadjane, P. Andjus and N. K. Logothetis, *Acs Chemical Neuroscience*, 2014, **5**, 360-369.
45. K. D. Verma, A. Forgacs, H. Uh, M. Beyerlein, M. E. Maier, S. Petoud, M. Botta and N. K. Logothetis, *Chemistry-a European Journal*, 2013, **19**, 18011-18026.
46. S. Gündüz, T. Savić, R. Pohmann, N. K. Logothetis, K. Scheffler and G. Angelovski, *ACS Sensors*, 2016, **1**, 483-487.
47. E. L. Que, E. J. New and C. J. Chang, *Chemical Science*, 2012, **3**, 1829-1834.
48. H. Xing, C. L. Zhang, G. Ruan, J. Zhang, K. Hwang and Y. Liu, *Analytical Chemistry*, 2016, **88**, 1506-1510.
49. B. A. Webb, M. Chimenti, M. P. Jacobson and D. L. Barber, *Nature Reviews Cancer*, 2011, **11**, 671-677.

50. N. Traverso, R. Ricciarelli, M. Nitti, B. Marengo, A. L. Furfaro, M. A. Pronzato, U. M. Marinari and C. Domenicotti, *Oxidative medicine and cellular longevity*, 2013, **2013**, 972913.
51. S. Mizukami, R. Takikawa, F. Sugihara, Y. Hori, H. Tochio, M. Walchli, M. Shirakawa and K. Kikuchi, *Journal of the American Chemical Society*, 2008, **130**, 794-+.
52. Y. Yuan, H. Sun, S. Ge, M. Wang, H. Zhao, L. Wang, L. An, J. Zhang, H. Zhang, B. Hu, J. Wang and G. Liang, *Acs Nano*, 2015, **9**, 761-768.
53. Y. Yuan, S. Ge, H. Sun, X. Dong, H. Zhao, L. An, J. Zhang, J. Wang, B. Hu and G. Liang, *ACS Nano*, 2015, **9**, 5117-5124.
54. H. Wang, K. R. Raghupathi, J. Zhuang and S. Thayumanavan, *ACS Macro Letters*, 2015, **4**, 422-425.
55. M. Buzhor, L. Avram, L. Frish, Y. Cohen and R. J. Amir, *Journal of Materials Chemistry B*, 2016, **4**, 3037-3042.
56. Z. Zheng, H. Sun, C. Hu, G. Li, X. Liu, P. Chen, Y. Cui, J. Liu, J. Wang and G. Liang, *Analytical Chemistry*, 2016, **88**, 3363-3368.
57. K. Tanaka, N. Kitamura and Y. Chujo, *Bioconjugate Chemistry*, 2011, **22**, 1484-1490.
58. K. Matsuo, R. Kamada, K. Mizusawa, H. Imai, Y. Takayama, M. Narazaki, T. Matsuda, Y. Takaoka and I. Hamachi, *Chemistry – A European Journal*, 2013, **19**, 12875-12883.
59. X. Yue, Z. Wang, L. Zhu, Y. Wang, C. Qian, Y. Ma, D. O. Kiesewetter, G. Niu and X. Chen, *Molecular Pharmaceutics*, 2014, **11**, 4208-4217.
60. A. Keliris, I. Mamedov, G. E. Hagberg, N. K. Logothetis, K. Scheffler and J. Engelmann, *Contrast Media & Molecular Imaging*, 2012, **7**, 478-483.
61. J. X. Yu, L. Liu, V. D. Kodibagkar, W. N. Cui and R. P. Mason, *Bioorganic & Medicinal Chemistry*, 2006, **14**, 326-333.
62. J.-X. Yu, V. D. Kodibagkar, L. Liu and R. P. Mason, *Nmr in Biomedicine*, 2008, **21**, 704-712.
63. X. Huang, G. Huang, S. Zhang, K. Sagiyama, O. Togao, X. Ma, Y. Wang, Y. Li, T. C. Soesbe, B. D. Sumer, M. Takahashi, A. D. Sherry and J. Gao, *Angewandte Chemie-International Edition*, 2013, **52**, 8074-8078.
64. M. Oishi, S. Sumitani and Y. Nagasaki, *Bioconjugate Chemistry*, 2007, **18**, 1379-1382.
65. S. Chen, Y. Yang, H. Li, X. Zhou and M. Liu, *Chemical Communications*, 2014, **50**, 283-285.
66. A. T. Preslar, F. Tantakitti, K. Park, S. Zhang, S. L. Stupp and T. J. Meade, *Acs Nano*, 2016, **10**, 7376-7384.
67. K. Tanaka, N. Kitamura, Y. Takahashi and Y. Chujo, *Bioorganic & Medicinal Chemistry*, 2009, **17**, 3818-3823.
68. D. Xie, T. L. King, A. Banerjee, V. Kohli and E. L. Que, *Journal of the American Chemical Society*, 2016, **138**, 2937-2940.
69. T. Nakamura, H. Matsushita, F. Sugihara, Y. Yoshioka, S. Mizukami and K. Kikuchi, *Angewandte Chemie-International Edition*, 2015, **54**, 1007-1010.
70. A. Bar-Shir, N. N. Yadav, A. A. Gilad, P. C. M. van Zijl, M. T. McMahon and J. W. M. Bulte, *Journal of the American Chemical Society*, 2015, **137**, 78-81.
71. C. Zhang, S. S. Moonshi, H. Peng, S. Puttick, J. Reid, S. Bernardi, D. J. Searles and A. K. Whittaker, *Acs Sensors*, 2016, **1**, 757-765.
72. Y. Takaoka, T. Sakamoto, S. Tsukiji, M. Narazaki, T. Matsuda, H. Tochio, M. Shirakawa and I. Hamachi, *Nature Chemistry*, 2009, **1**, 557-561.